

## Interparticle force between different types of nematic colloids

Kuniyoshi Izaki and Yasuyuki Kimura\*

*Department of Physics, School of Sciences, Kyushu University, 6-10-1 Hakozaki, Higashi-ku, Fukuoka 812-8581, Japan*

(Received 16 February 2013; revised manuscript received 25 April 2013; published 20 June 2013)

We have studied the interparticle force between colloidal particles with three different types of defects in nematic liquid crystal by dual-beam optical tweezers. The force between a dipole (D)- and a Saturn-ring (S)-type particle at large interparticle distance  $R$  is proportional to  $R^{-4.95 \pm 0.05}$ . The force between a D- and a planar (P)-type particle and that between an S- and a P-type particle are, respectively, proportional to  $R^{-5.04 \pm 0.08}$  and  $R^{-5.78 \pm 0.13}$ . The observed dependence of the interparticle force on  $R$  at large  $R$  is in agreement with that predicted by electrostatic analogy. The topological quadrupole moments for S and P particles are evaluated from experimental data. We have also studied the force curves in oblique arrangement against the far-field director for respective pairs. The experimental force curves at large  $R$  quantitatively agree with those predicted by electrostatic analogy, but they always become attractive at small  $R$  due to the reorientation and deformation of defects. The force profiles for the S-P pair are also compared with those obtained by the recent numerical simulation.

DOI: [10.1103/PhysRevE.87.062507](https://doi.org/10.1103/PhysRevE.87.062507)

PACS number(s): 61.30.Jf, 61.30.Gd, 82.70.Dd

### I. INTRODUCTION

The interaction between colloidal particles in isotropic liquids has been intensively studied from fundamental and practical points of view. For micrometer-sized colloids, van der Waals and electrostatic interactions play important roles for the stability of colloidal dispersions [1,2]. Recently, nontrivial interactions between colloids have been studied in so-called structured fluids such as polymer solutions [1,2] and liquid crystals [3–7]. In these systems, their mesoscopic structures induce characteristic interaction between the dispersed particles.

In this study, we focus colloidal dispersion in nematic liquid crystal (NLC), which is often called nematic colloids. NLC is anisotropic fluid in which the rotational symmetry is broken and anisotropic constituent molecules arrange uniaxially [8–10]. Their average direction is represented by a unit vector called a director. Since the local distortion of the director field costs energy, the orientational elasticity appears in NLC. When a colloidal particle is dispersed in NLC, the particle itself becomes a topological defect to the orientational order of the nematic medium. Moreover, an additional defect emerges near the particle to satisfy global boundary conditions. Depending on the strength and the direction of the anchoring of NLC at the particle's surface, and the size of the particle, three types of particle-defect pairs have been reported [5–7,11–13]. They are respectively called “dipole” (D), “Saturn-ring” (S), and “planar quadrupole” (P) particles.

In a D particle [Fig. 1(a)], a hyperbolic hedgehog defect emerges near the particle. The line connecting the center of the particle and the accompanying defect is parallel to the director field far from the particle. In an S particle [Fig. 1(b)], a disclination loop appears above the equator of the particle. The plane containing the disclination loop is perpendicular to the far-field director. The D and S particles are usually observed for micrometer-sized particles with homeotropic surface anchoring, where NLC aligns perpendicular to the

particle's surface. In the case of strong homeotropic anchoring and a large particle, the D configuration is energetically more favorable [11]. In a P particle [Fig. 1(c)], the boundary condition at the particle's surface is planar and two surface defects known as “boojums” are induced at the poles of the particle [13]. The line connecting two boojums is parallel to the far-field director. As shown in Fig. 1, these three types of particle-defect pairs can be distinguished from each other under a polarizing microscope.

The interaction between the particles with such characteristic defects is different from that in isotropic fluids. Due to the long-range and anisotropic nature of the orientational order in NLC, the interaction between colloids in NLC is also long range and anisotropic. An interparticle force  $F$  depends on the symmetry of the particle's configuration. According to the electrostatic analogy of the nematic field [7], a D particle exhibits the interaction in dipolar nature, and an S and a P particle exhibit that in quadrupolar nature. Therefore, the interaction between two D particles is a dipolar-dipolar one, and the dependence of  $F$  on the interparticle distance  $R$  is  $F \propto R^{-4}$ . This dependence at large  $R$  has been confirmed quantitatively by experiments [14–20] and computer simulations [11,12,21–24]. On the other hand,  $F$  between two P particles is repulsive along the direction parallel to the far-field director [4,7,16,25–30], and  $F \propto R^{-6}$ . Although the dependence of  $F$  on  $R$  at large  $R$  is intensively studied, the entire profile of the force curve has not been studied much.

In this study, we measured the interparticle force  $F$  between different types of nematic colloids by dual-beam optical tweezers. We also studied the dependence of  $F$  on the angle  $\theta$  between the line connecting the centers of two particles and far-field director. The experimental results are directly compared with the theoretical force curves obtained by electrostatic analogy or by computer simulations. According to the electrostatic analogy, the interparticle force along the line connecting the centers of two particles  $F_r$  between D, S, and P particles are respectively expected to be  $F_r^{DS} \propto R^{-5}$ ,  $F_r^{DP} \propto R^{-5}$ , and  $F_r^{PS} \propto R^{-6}$ , which will be discussed later [7,28]. The information on the anisotropy of interparticle force obtained in this study is valuable toward the design of complex

\*kimura@phys.kyushu-u.ac.jp

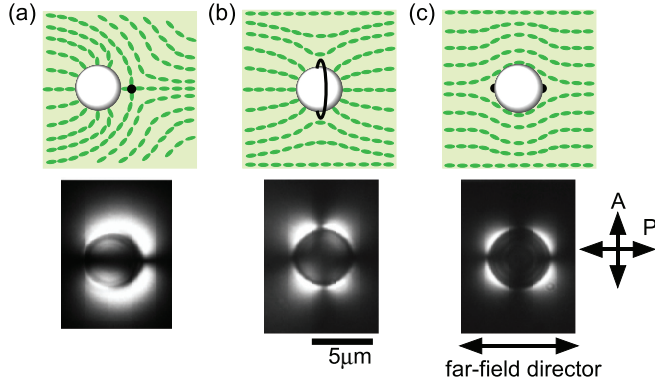


FIG. 1. (Color online) Schematic figures and polarizing microscope images (cross-Nicoles) of particle-defect pairs in NLC: (a) dipole, (D) particle; (b) Saturn ring, (S) particle; (c) planar quadrupole, (P) particle. In upper figures, ellipsoids represent LC molecules. In the lower images, the direction of background nematic field is parallel to the horizontal line. The black parts correspond to the regions where the local director is parallel or perpendicular to the far-field director.

two-dimensional microstructures composed of different types of nematic colloids [31–33].

## II. EXPERIMENT

In this study, we used dual-beam optical tweezers to align two particles along the oblique direction  $\theta$  against the far-field director and to measure the interparticle force. This method can escape some difficulties in the frequently used free-release method [14,18,31,33]: the hydrodynamic effect at small interparticle distance [34] and estimation of effective viscosity of the nematic medium [33]. Especially in the case of particles approaching in oblique direction against the far-field director, it is difficult to fix the approaching angle in general [33].

On the contrary, in the optical tweezing method, two crucial effects have been reported. One is the optical alignment of the director under a focused intense laser beam [35,36]. The other is the local variation of the order parameter due to the local laser heating [37]. We used a small laser power for the force measurement to minimize the optical deformation of the local director field. The local variation of the director originating from the laser has not been observed under a polarizing microscope. We also used a liquid crystal (LC) with higher  $N-I$  transition temperature (ca. 50 °C) to eliminate the notable variation of order parameters due to the local heating effect. Judging from our previous studies [19,20,34,38], the serious influence of optical deformation on force measurement is apparent only at a very small distance where the repulsive component is dominant, and the measurement error is estimated within 10% in that region.

We dispersed polystyrene latex particles with radius  $a = 2.55 \pm 0.1 \mu\text{m}$  (Magsphere, Inc.) in a nematic liquid crystal MJ032358 (Merck, Japan). The refractive index of the particles is 1.6, and the extraordinary and ordinary refractive indices,  $n_e$  and  $n_o$ , of the LC are  $n_e = 1.5$  and  $n_o = 1.46$ ,

respectively. Therefore we can stably trap the particles in any direction.

The surface anchoring of the particles is controlled by coating their surfaces with an appropriate surfactant [39]. The homeotropic anchoring is realized by octadecyldimethyl (3-trimethoxysilylpropyl) ammonium chloride (DMOAP, Gelest, Inc.), and the planar anchoring is accomplished by 3-methylaminopropyl trimethoxysilane (MAP, Gelest, Inc.). We prepared the dispersion of the particles with different surface alignments separately and mixed them just before injection into a sample cell at nematic phase. The formation of D and S particles is usually controlled by the thickness of a cell, because an S configuration is more stable than a D configuration in thinner cells [18]. However, we controlled the configuration of homeotropic particles by the concentration of DMOAP and used a 30- $\mu\text{m}$ -thick cell in this study. According to the previous studies [20,40–42], the confinement in thin cells makes the interparticle force short ranged. Since we studied the interaction of D particles [20], we expect to eliminate this confinement effect from our experimental results using thick cells. However, the inhomogeneity of coating by surfactant results in the variation of anchoring on the surface. This often distorted the disclination ring of an S particle.

The cell surfaces were spin-coated with polyimide and rubbed unidirectionally to attain the planar alignment of LC. A 30- $\mu\text{m}$ -thick film was used as a space of a LC cell. When the surface alignment of a particle is homeotropic and that of the cell surface is planar, the mismatch between two boundary conditions induces the repulsion between the particle and the cell [28]. Therefore D and S particles tend to cite near the center of the cell. On the contrary, the boundary condition of P particles and that of the cell surface is the same. This induces the attraction or no repulsion between the particles and the cell surface. This promotes the adsorption of P particles to cell surfaces considerably. In order to avoid this unexpected adsorption, the free P particles are forced to bind D particles using optical tweezers before they attach to cell surfaces. Such a pair stably floats in NLC. In this study, we used the same particles for force measurement to evaluate the topological quadrupole moments of nematic colloids under the same condition.

The experimental details of our force measurement method have been reported elsewhere [19,20]. We used a Nd:YVO<sub>4</sub> laser (Spectra Physics, wavelength 1064 nm) for dual-beam optical tweezers. The laser beams were introduced into an inverted fluorescence microscope (TE2000U, Nikon) and focused using a 100 $\times$  oil immersion objective lens (Plan Fluor, N.A. = 1.3, Nikon). In this experiment, we approach one particle obliquely against the direction of the far-field director using the optical tweezers. The position of the beam was controlled by two Galvano mirrors (model 6450, Cambridge Technology, Inc.) driven by a two-channel function generator (model 1946, NF Corp.).

## III. THEORETICAL PREDICTION ON INTERPARTICLE FORCE BY ELECTROSTATIC ANALOGY

According to the electrostatic analogy [4,7,25,28], the interparticle interaction between a dipolar and a quadrupolar

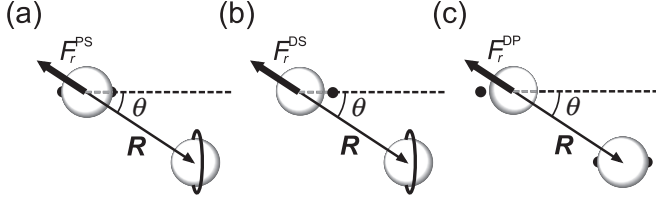


FIG. 2. Arrangements of two particles used for force measurement: (a) P-S ( $Q_s > 0$ ,  $Q_p < 0$ ), (b) D-S ( $d < 0$ ,  $Q_s > 0$ ), (c) D-P ( $d > 0$ ,  $Q_p < 0$ ).  $|\mathbf{R}|$ : interparticle distance,  $\theta$ : oblique angle,  $\mathbf{F}_r$ : radial force.

particle  $U_{dQ}$  and two quadrupolar particles  $U_{QQ}$  are respectively given as

$$U_{dQ} = \frac{16\pi K}{R^4} [2\{(\mathbf{Q}_i^{(1)} : \mathbf{u}) \cdot \mathbf{d}_i^{(2)} - (\mathbf{Q}_i^{(2)} : \mathbf{u}) \cdot \mathbf{d}_i^{(1)}\} - 5\{(\mathbf{Q}_i^{(1)} : \mathbf{u} : \mathbf{u})(\mathbf{u} \cdot \mathbf{d}_i^{(2)}) - (\mathbf{Q}_i^{(2)} : \mathbf{u} : \mathbf{u})(\mathbf{u} \cdot \mathbf{d}_i^{(1)})\}], \quad (1)$$

$$U_{QQ} = -\frac{20\pi K}{3R^5} [2(\mathbf{Q}_i^{(1)} : \mathbf{Q}_i^{(2)}) + 35(\mathbf{Q}_i^{(1)} : \mathbf{u} : \mathbf{u}) \cdot (\mathbf{Q}_i^{(2)} : \mathbf{u} : \mathbf{u}) - 20(\mathbf{Q}_i^{(1)} : \mathbf{u} : \mathbf{Q}_i^{(2)} : \mathbf{u})], \quad (2)$$

where  $\mathbf{d}_i^{(i)}$  and  $\mathbf{Q}_i^{(i)}$  are the dipole-moment and quadrupole-moment of the  $i$ th particle determined by the surface density of the transverse director field, and  $\mathbf{u} = \mathbf{R}/R$  is the unit vector connecting the centers of two particles. Although Eq. (2) has already been derived in Ref. [28], we derive Eq. (1) from the multipole expansion of the interparticle interaction following Ref. [28]. In our measurement condition as shown in Fig. 2, the forces along the line connecting the centers of two particles  $F_r$  between D, S, and P particles are respectively given as [43]

$$F_r^{DS} = -\frac{128\pi K}{R^5} |d| Q_s (5 \cos^2 \theta - 3) \cos \theta, \quad (3)$$

$$F_r^{DP} = +\frac{128\pi K}{R^5} |d| Q_p (5 \cos^2 \theta - 3) \cos \theta, \quad (4)$$

$$F_r^{PS} = +\frac{400\pi K}{3R^6} Q_p Q_s (35 \cos^4 \theta - 30 \cos^2 \theta + 3), \quad (5)$$

where  $d$  is the dipole moment,  $Q_s$  and  $Q_p$  are the quadrupolar moment, for the S and P particle, respectively, and  $\theta$  is the angle between the line connecting the centers of the two particles and the far-field director. Since  $Q_s > 0$  and  $Q_p < 0$  [33,44],  $F_r$  at  $\theta = 0$  are attractive in all the above cases. The applicability of electrostatic analogy at large  $R$  for  $\theta = 0$  has already been studied experimentally by a free-release method in D-S [31] and P-S pairs [33].

#### IV. INTERPARTICLE FORCE ALONG THE FAR-FIELD DIRECTOR ( $\theta = 0$ )

##### A. P-S particles

Figure 3(a) shows the dependence of the interparticle force  $F$  between P and S particles on the reduced interparticle distance  $D (=R/a)$ . The positive and negative values of  $F$  respectively represent the repulsive and attractive forces. The maximum attractive force is 8.9 pN at  $D = 2.37$ , which is smaller than that between D-D particles ( $\sim 25$  pN) [20]. The

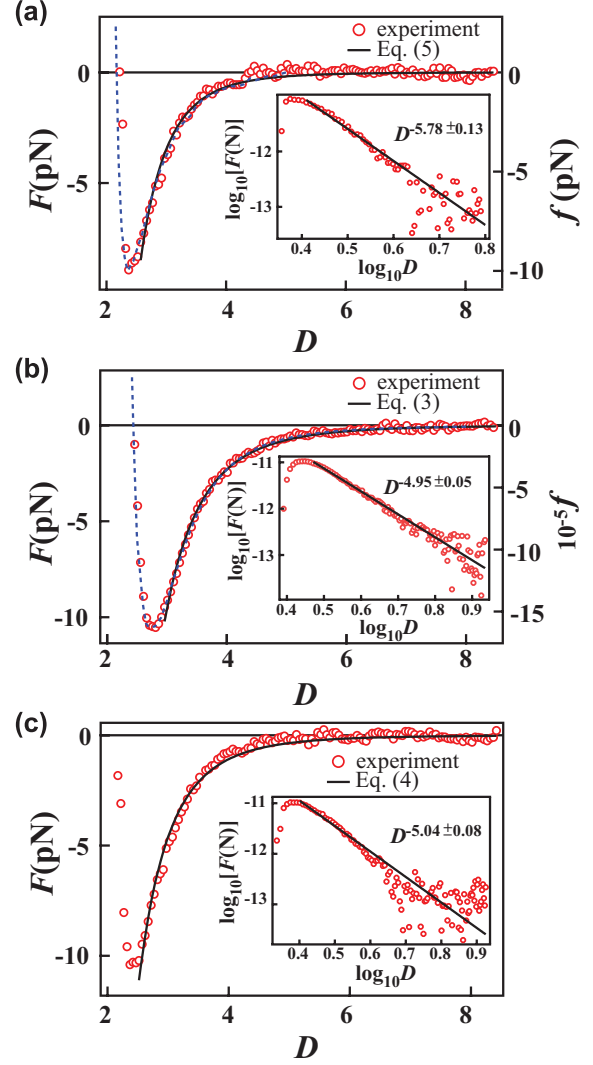


FIG. 3. (Color online) Dependence of the interparticle force  $F$  between different types of nematic colloids at  $\theta = 0$  on the reduced interparticle distance  $D = R/a$ : (a) P-S particles, (b) D-S particles, and (c) D-P particles. Empty circles are experimental data  $F$ . Solid lines are respectively the best-fitted curve of Eqs. (5), (3), and (4). The dependence of  $F$  on  $D$  is also plotted in logarithmic scale in the inset. The lines in the insets are the best-fitted curves of the power law. Broken lines in (a) and (b) are theoretical simulation data  $f$  respectively taken from Refs. [44] and [38].

equilibrium separation where  $F = 0$  is 2.22 and is smaller than 2.4 in the D-D case. This is due to that a defect in P-particle sites on the surface of the particle.

The attractive component of  $F$  at large  $D$  is well described by electrostatic analogy. The best-fitted curve of a power law to the data for  $D > 3$  is shown as a solid line in Fig. 3(a) and is also shown in the inset. The best-fitted exponent is  $-5.78 \pm 0.13$  and agrees with  $-6$ , as predicted in Eq. (5). On the other hand, there is short-range repulsive component, which is similar to that reported for a D-D pair [14,17,19,20]. This repulsive component originates from the nonlinear deformation of the nematic field, including the deformation of a boojum defect existing between the particles.

Since the finite size effect of the particles is not taken into account in electrostatic analogy, the experimental force curve at small  $D$  cannot be explained by electrostatic analogy alone [17]. However, the numerical simulation of the nematic field, including two particles, enables us to evaluate the whole force curve, including the deformation of defects. The theoretically calculated force curve  $f$  by Eskandari *et al.* [44] is plotted as a broken line in Fig. 3(a) by adjusting the maximum attractive force to the experimental force. There was agreement with the experimental data fairly well over the entire  $D$ , i.e., the force profile at small  $D$  and the distance where the force exhibits a maximum attractive force.

### B. D-S particles

Figure 3(b) shows the dependence of  $F$  between D and S particles on  $D$ . The maximum attractive force is 10.05 pN at  $D = 2.81$ . The maximum force and the corresponding interparticle distance are larger than those for P-S pairs. The equilibrium separation is 2.44 and is similar to that in a D-D pair.

The best-fitted curve of a power law to the data for  $D > 3$  is shown as a solid line in Fig. 3(b) and in the inset. The obtained exponent is  $-4.95 \pm 0.05$  and shows good agreement with  $-5$ , as predicted in Eq. (3). The theoretically calculated force curve  $f$  by Kishita *et al.* [38] is plotted as a broken line in Fig. 3(b) by adjusting the maximum attractive force to the experimental one. The agreement with experimental data is fairly good over the whole  $D$ .

### C. D-P particles

Figure 3(c) shows the dependence of  $F$  between D and P particles on  $D$ . The maximum attractive force is 10.30 pN and is almost same as that in a D-S pair, but the corresponding interparticle distance is  $D = 2.42$  and is smaller than that in the D-S pair. Comparing those force curves at large  $D$ , the magnitude  $|F|$  at the same  $D$  is  $|F^{DS}| > |F^{DP}|$ . However, the equilibrium distance at which  $F = 0$  is larger in the D-S pair. This indicates that the repulsive component is weaker in the D-P pair. This is the reason why the maximum attractive forces for those pairs exhibit almost similar values.

The best-fitted curve of a power law to the data for  $D > 3$  is drawn as a solid line in Fig. 3(c) and in the inset. The obtained exponent is  $-5.04 \pm 0.08$  and makes good agreement with  $-5$ , as predicted in Eq. (4). As far as we know, the simulation of the force curve for D-P pairs has not been reported.

### D. Evaluation of topological quadrupole moments $|Q_s|$ and $|Q_p|$

We evaluate topological quadrupole moments for S and P particles from the experimental data in the following way. We made the fitting of Eqs. (3) and (4) with  $\theta = 0$  to experimental force curves by fixing the exponent to  $-5$  and obtained the ratio  $|Q_s|/|Q_p|$ . For a P-S pair, we fitted Eq. (5) with  $\theta = 0$  by fixing the exponent to  $-6$  and obtained  $|Q_s|, |Q_p|$  using the effective elastic constant  $K = 7.2$  pN reported previously [20]. From these two values, we obtained  $|Q_s| = 0.47a^3$  and  $|Q_p| = 0.21a^3$ , where  $a$  is the radius of a particle.

According to Ref. [44], the obtained value of  $|Q_s|$  in this experiment is close to that estimated theoretically ( $0.4a^3$ ) [45] and experimentally ( $0.5a^3$ ) [33]. Although the values of  $|Q_p|$  obtained by previous experiments listed in Ref. [44] are largely dispersed ( $0.17 \sim 0.36a^3$ ), the obtained  $|Q_p|$  in this study is within this range. One of the reasons for the dispersion of data is partially due to the difference in the strength of surface anchoring. According to the recent theoretical study [30], the defect structure in the P particle depends on the anchoring strength and temperature, and its interaction also depends on the defect structure.

## V. INTERPARTICLE FORCE ALONG THE OBLIQUE DIRECTION AGAINST THE FAR-FIELD DIRECTOR ( $\theta \neq 0$ )

When two particles are obliquely aligned to the far-field director as shown in Fig. 2, the interparticle force  $F$  can be decomposed into two components: one is radial and the other is polar (azimuthal). In the following, we only discuss the radial component  $F_r$ .

### A. D-D particles

Although the interparticle force  $F_r$  between D-D particles at  $\theta = 0$  has intensively been studied [14,17,19,20], the dependence of force curves on  $\theta$  has not been studied much [15]. Before studying  $F_r$  between nematic colloids in different configurations, we discuss the experimental force curve  $F_r$  for D-D particles and compare the prediction based on electrostatic analogy for  $\theta \neq 0$ .

According to the electrostatic analogy [7,28], the dependence of  $F_r$  on  $\theta$  is given as  $F_r(\theta) = F_r(0)(3 \cos^2 \theta - 1)/2$ . As shown in Fig. 4,  $F_r$  decreases with increase of  $\theta$  at large  $D$ , and changes its sign to positive near  $\theta \sim 60^\circ$ . This behavior is qualitatively consistent with the theoretical prediction;  $F_r$  changes its sign from negative to positive at  $\theta = 54.7^\circ$ . However,  $F_r$  at small  $D$  is negative even for large  $\theta$ . Since we fixed the particle by a laser beam of a few micrometers in diameter, this allows the free reorientation of the dipole around the beam axis. The interaction between particles in a nonaxial

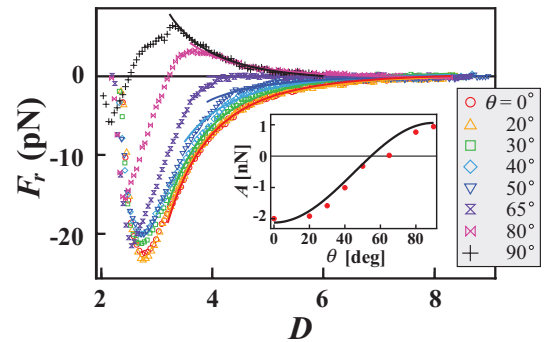


FIG. 4. (Color online) Dependence of the radial component of the interparticle force  $F_r$  between D-D particles on the reduced interparticle distance  $D$  at various angles  $\theta$ . The solid lines are the best-fitted ones of power law  $F_r = A/D^4$ . The dependence of the magnitude  $A$  on  $\theta$  is shown in the inset. The solid curve in the inset is the best-fitted curve of  $C(\cos^2 \theta - 1/3)$ .

arrangement cannot be discussed by electrostatic analogy with uniaxial symmetry [7].

Except for the small  $D$  region, we can fit the force curves for  $D \geq 3.5 \sim 4$  with  $F_r = A/D^4$ , drawn as solid curves in Fig. 4. The dependence of the best-fitted values of  $A$  on  $\theta$  is also shown in the inset of Fig. 4. The dependence is theoretically predicted as  $A(\theta) = C(\cos^2 \theta - 1/3)$  ( $C$ : const.). The overall dependence semiquantitatively agrees with the theoretical curve, as shown in a solid line in the inset of Fig. 4. However, the discrepancy is large in the small  $F_r$  region. In this  $\theta$  region, the range of  $D$  where the relation  $F_r \propto D^{-4}$  is applicable becomes narrower. In conclusion,  $F_r$  at large  $D$  is semiquantitatively consistent with the prediction by electrostatic analogy.

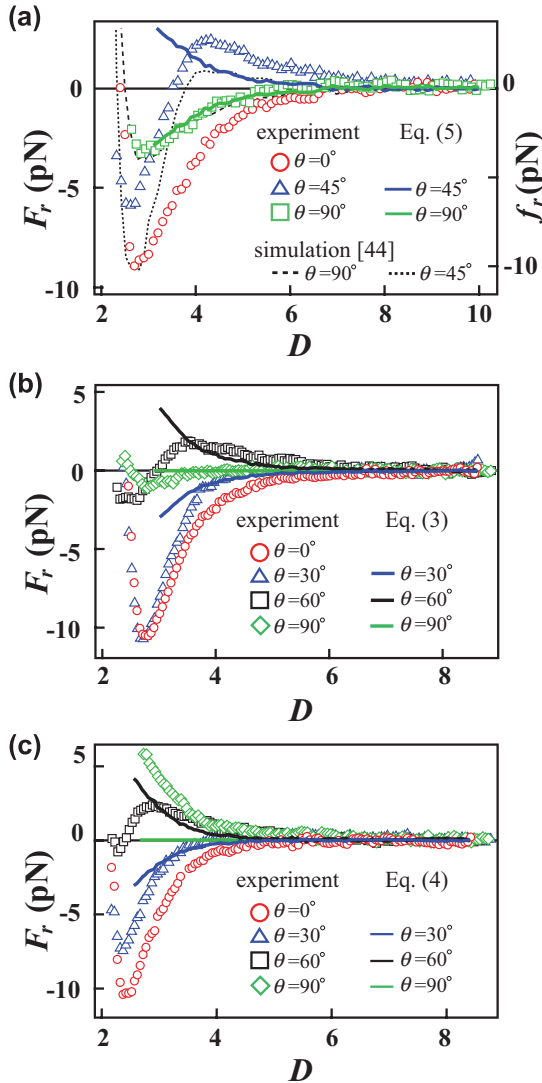


FIG. 5. (Color online) Dependence of the radial component of the interparticle force  $F_r$  between different types of nematic colloids on the reduced interparticle distance  $D$  at various angles  $\theta$ : (a) P-S particles, (b) D-S particles, and (c) D-P particles. The predicted force curves by Eqs. (5), (3), and (4) with the experimental data  $F_r(\theta = 0)$  are respectively drawn in solid lines. The thin broken lines in (a) are the force curves  $f_r$  obtained by computer simulation [44].

## B. P-S particles

Figure 5(a) shows the force curves between P and S particles at  $\theta = 0^\circ$ ,  $45^\circ$ , and  $90^\circ$ . At large  $D$ ,  $F_r$  is negative at  $\theta = 0^\circ$  and  $90^\circ$ , and is positive at  $\theta = 45^\circ$ . We can predict the force curve at large  $D$  by electrostatic analogy with Eq. (5) and the experimental data at  $\theta = 0$ . The expected force curves,  $F_r(\theta) = F_r(0)(35 \cos^4 \theta - 30 \cos^2 \theta + 3)/8$ , at  $\theta = 45^\circ$  and  $90^\circ$ , are shown as solid lines in Fig. 5(a). Although the agreement is fairly good at  $\theta = 90^\circ$ , the agreement is only qualitative at  $\theta = 45^\circ$ .

The experimental force curves are also compared with the theoretical ones  $f_r$  obtained by recent numerical simulation [44]. The theoretical force curves are scaled to adjust the maximum attractive force of experimental data at  $\theta = 0^\circ$ , as shown in Fig. 3(a). The agreement is fairly good at  $\theta = 90^\circ$  for the whole range of  $D$ . Although the overall profile at  $\theta = 45^\circ$  qualitatively agrees, the magnitude differs largely from experimental data. On the contrary, the agreement between the simulation data and the electrostatic prediction at large  $D$  is fairly good even at  $\theta = 45^\circ$ .

There are some possible reasons for the discrepancy between experiment and electrostatic analogy at  $\theta = 45^\circ$ . One is the nonideal defect structure probably due to the inhomogeneity of the surface anchoring. The other is the distortion of defects at small  $D$  and the difficulty in keeping the particles' positions within two dimensions. The polarizing microscope image during the force measurement for the P-S pair is shown in Fig. 6. With decreasing  $D$ , the line connecting two boojums in the P particle and the disclination ring in the S particle tilts from their original positions. The distortion of defects relates the displacement of topological charge, and the electrostatic analogy cannot be applied to this case.

Although the simulation at  $\theta = 45^\circ$  reproduces the deformation of defects fairly well, as schematically shown in Fig. 6(b), the details seem to be different from each other: the position of the boojums and that of the disclination ring. Such discrepancy between experiment and simulation has been also reported for P-P particles [30]. Although the overall dependence on  $\theta$  qualitatively agrees, the relative magnitude does not agree with the experimental data [16].

## C. D-S particles

The force  $F_r$  between D-S particles at  $\theta = 0^\circ$ ,  $30^\circ$ ,  $60^\circ$ , and  $90^\circ$  is shown in Fig. 5(b). According to Eq. (3),  $F_r$  is

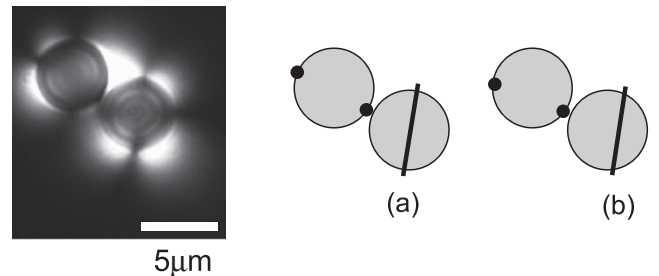


FIG. 6. Polarizing microscope image of a P-S pair under force measurement (cross-Nicoles). The arrangement of boojums and a disclination ring in (a) experiment and (b) simulation (Fig. 4 in Ref. [44]) are also schematically drawn.

attractive for  $0 < \theta < 39.3^\circ$ , repulsive for  $39.3^\circ < \theta < 90^\circ$ , and zero at  $\theta = 90^\circ$ . The expected force curves calculated by Eq. (3) with the experimental force curve at  $\theta = 0$ ,  $F_r(\theta) = F_r(0)(5 \cos^2 \theta - 3) \cos \theta/2$ , are plotted as solid lines in Fig. 5(b). The calculated curves exhibit quantitative agreement with experimental curves for  $D \geq 3.5$ . However, at small  $D$ , all forces exhibit negative values, even for  $39.3^\circ < \theta < 90^\circ$ . This is also due to the reorientation of particles or deformation of defects to minimize the interparticle energy. Since there is no simulation force curve of  $\theta \neq 0$  corresponding to our experimental one as far as we know, we cannot further discuss the force curve in detail.

#### D. D-P particles

The force  $F_r$  between D-P particles at  $\theta = 0^\circ, 30^\circ, 60^\circ$ , and  $90^\circ$  are shown in Fig. 5(c). The theoretically expected dependence is the same as in a D-S pair. The expected force curves calculated by Eq. (4) with the experimental force curve at  $\theta = 0^\circ$  are plotted as solid lines in Fig. 5(c). Except  $\theta = 90^\circ$ , the agreement between theoretical prediction and experiment at large  $D$  is qualitatively similar to that for a D-S pair. However, the interparticle distance where the attractive force exhibits a maximum value monotonously decreases with  $\theta$ , in contrast to the D-S pair. Although  $F_r$  is expected to be zero at  $\theta = 90^\circ$ , observation reveals a large positive value. This seems to relate to the fact that there is no defect between the particles at  $\theta = 90^\circ$  in the D-P pair [Fig. 2(c)]. The bare interaction between two particles for the D-P pair increases the repulsive component effectively, but such a finite size effect is not taken into account in electrostatic analogy. Thus the theoretical force curve by computer simulation is necessary

to discuss the reason for the discrepancy at  $\theta = 90^\circ$  in more detail.

#### VI. CONCLUSIONS

We studied the interparticle force between nematic colloids in different configurations by dual-beam optical tweezers. For  $\theta = 0$ , the asymptotic behavior of the force curves at large  $R$  make good agreement with that predicted by electrostatic analogy. The entire profile also exhibits good quantitative agreement with the computer simulation for D-S and P-S pairs. For the  $\theta \neq 0$  case, most of the force curves we studied show quantitative agreement with the electrostatic ones at large  $R$ . However, the discrepancy is large for the P-S pair at  $\theta = 45^\circ$  and the D-P pair at  $\theta = 90^\circ$ . To discuss our entire experimental force curve quantitatively, it is necessary to calculate the theoretical force curve by computer simulation.

The anisotropic interaction in nematic colloids is analogous to the anisotropic nature of molecular orbits. Therefore it is expected that various kinds of complex assemblies, similar to real molecules, can be realized. The characteristic anisotropic interparticle force between different nematic colloids will open a way of constructing more complex self-assembled structures in micrometer scale beyond the simple regular structure similar to colloidal crystals [31–33].

#### ACKNOWLEDGMENTS

The authors thank B. Fukai and T. Uramoto at Kyushu University for their technical assistance. They also thank Merck Japan, Ltd., for providing the liquid crystal samples. This work was supported by a Grant-in-Aid for Scientific Research, KAKENHI, from JSPS.

- 
- [1] W. B. Russel, D. A. Saville, and W. R. Schowalter, *Colloidal Dispersions* (Cambridge University Press, Cambridge, 1989).
  - [2] J. N. Israelachvili, *Intermolecular and Surface Forces*, 2nd ed. (Academic, London, 1992).
  - [3] E. M. Terentjev, *Phys. Rev. E* **51**, 1330 (1995).
  - [4] S. Ramaswamy, R. Nityananda, V. A. Raghunathan, and J. Prost, *Mol. Cryst. Liq. Cryst.* **288**, 175 (1996).
  - [5] R. W. Ruhwandl and E. M. Terentjev, *Phys. Rev. E* **56**, 5561 (1997).
  - [6] P. Poulin, H. Stark, T. C. Lubensky, and D. A. Weitz, *Science* **275**, 1770 (1997).
  - [7] T. C. Lubensky, D. Petthey, N. Currier, and H. Stark, *Phys. Rev. E* **57**, 610 (1998).
  - [8] P. G. de Gennes and J. Prost, *The Physics of Liquid Crystals*, 2nd ed. (Oxford, New York, 1993).
  - [9] M. Kleman and O. D. Lavrentovich, *Soft Matter Physics: An Introduction* (Springer-Verlag, New York, 2003).
  - [10] P. Oswald and P. Pieranski, *Nematic and Cholesteric Liquid Crystals: Concepts and Physical Properties Illustrated by Experiments* (CRC Press, Boca Raton, FL, 2005).
  - [11] H. Stark, *Phys. Rep.* **351**, 387 (2001).
  - [12] J. Fukuda, *J. Phys. Soc. Jpn.* **78**, 041003 (2009).
  - [13] P. Poulin and D. A. Weitz, *Phys. Rev. E* **57**, 626 (1998).
  - [14] P. Poulin, V. Cabuil, and D. A. Weitz, *Phys. Rev. Lett.* **79**, 4862 (1997).
  - [15] M. Yada, J. Yamamoto, and H. Yokoyama, *Phys. Rev. Lett.* **92**, 185501 (2004).
  - [16] I. I. Smalyukh, O. D. Lavrentovich, A. N. Kuzmin, A. V. Kachynski, and P. N. Prasad, *Phys. Rev. Lett.* **95**, 157801 (2005).
  - [17] C. M. Noël, G. Bossis, A.-M. Chaze, F. Giulieri, and S. Laciš, *Phys. Rev. Lett.* **96**, 217801 (2006).
  - [18] M. Škarabot, M. Ravnik, S. Žumer, U. Tkalec, I. Poberaj, D. Babič, N. Osterman, and I. Muševič, *Phys. Rev. E* **76**, 051406 (2007).
  - [19] K. Takahashi, M. Ichikawa, and Y. Kimura, *Phys. Rev. E* **77**, 020703(R) (2008).
  - [20] N. Kondo, Y. Iwashita, and Y. Kimura, *Phys. Rev. E* **82**, 020701(R) (2010).
  - [21] J. I. Fukuda, H. Stark, M. Yoneya, and H. Yokoyama, *Phys. Rev. E* **69**, 041706 (2004).
  - [22] J. Fukuda, H. Stark, M. Yoneya, and H. Yokoyama, *Mol. Cryst. Liq. Cryst.* **435**, 63 (2005).
  - [23] C. Zhou, P. Yue, and J. J. Feng, *Langmuir* **24**, 3099 (2008).
  - [24] K. S. Korolev and D. R. Nelson, *Phys. Rev. E* **77**, 051702 (2008).
  - [25] R. W. Ruhwandl and E. M. Terentjev, *Phys. Rev. E* **55**, 2958 (1997).

- [26] S. Grollau, N. L. Abbott, and J. J. de Pablo, *Phys. Rev. E* **67**, 011702 (2003).
- [27] S. Grollau, E. B. Kim, O. Guzman, N. L. Abbott, and J. J. de Pablo, *J. Chem. Phys.* **119**, 2444 (2003).
- [28] V. M. Pergamenschik and V. A. Uzunova, *Condens. Matter Phys.* **13**, 33602 (2010).
- [29] M. R. Mozaffari, M. Babadi, J.-I. Fukuda, and M. R. Ejthadi, *Soft Matter* **7**, 1107 (2011).
- [30] M. Tasinkevych, N. N. Silverstre, and M. M. Telo da Gama, *New J. Phys.* **14**, 073030 (2012).
- [31] U. Ognysta, A. Nych, V. Nazarenko, I. Mušević, M. Škarabot, M. Ravnik, S. Žumer, I. Poberaj, and D. Babič, *Phys. Rev. Lett.* **100**, 217803 (2008).
- [32] U. Ognysta, A. Nych, V. Nazarenko, M. Škarabot, and I. Mušević, *Langmuir* **25**, 12092 (2009).
- [33] U. M. Ognysta, A. B. Nych, V. A. Uzunova, V. M. Pergamenschik, V. G. Nazarenko, M. Škarabot, and I. Mušević, *Phys. Rev. E* **83**, 041709 (2011).
- [34] K. Takahashi, M. Ichikawa, and Y. Kimura, *J. Phys.: Condens. Matter* **20**, 075106 (2008).
- [35] I. Mušević, M. Škarabot, D. Babič, N. Osterman, I. Poberaj, V. Nazarenko, and A. Nych, *Phys. Rev. Lett.* **93**, 187801 (2004).
- [36] M. Škarabot, M. Ravnik, D. Babič, N. Osterman, I. Poberaj, S. Žumer, I. Mušević, A. Nych, U. Ognysta, and V. Nazarenko, *Phys. Rev. E* **73**, 021705 (2006).
- [37] S. A. Tatarikova, D. R. Burnham, A. K. Kirby, G. D. Love, and E. M. Terentjev, *Phys. Rev. Lett.* **98**, 157801 (2007).
- [38] T. Kishita, N. Kondo, K. Takahashi, M. Ichikawa, J.-I. Fukuda, and Y. Kimura, *Phys. Rev. E* **84**, 021704 (2011).
- [39] F. J. Kahn, *Appl. Phys. Lett.* **22**, 386 (1973).
- [40] M. Vilfan, N. Osterman, M. Čopič, M. Ravnik, S. Žumer, J. Kotar, D. Babič, and I. Poberaj, *Phys. Rev. Lett.* **101**, 237801 (2008).
- [41] J. I. Fukuda and S. Žumer, *Phys. Rev. E* **79**, 041703 (2009).
- [42] S. B. Chernyshuk and B. I. Lev, *Phys. Rev. E* **81**, 041701 (2010).
- [43] These equations differ from those derived from the discussion in Ref. [5]. This discrepancy is due to the difference of the coefficients in the series expansion of the nematic field.
- [44] Z. Eskandari, N. M. Silvestre, M. Tasinkevych, and M. M. Telo da Gama, *Soft Matter* **8**, 10100 (2012).
- [45] V. M. Pergamenschik and V. A. Uzunova, *Phys. Rev. E* **83**, 021701 (2011).